

Article

# Dice-Like Nanostructure of a CuS@PbS Composite for High-Performance Supercapacitor Electrode Applications

Ikkurthi Kanaka Durga <sup>1</sup>, S. Srinivasa Rao <sup>2</sup>, Jin-Woo Ahn <sup>2</sup>, Tae-Yong Park <sup>1</sup>, Bak Jin-Soo <sup>1</sup>, Cho-In Ho <sup>1</sup>, K. Prabakar <sup>1</sup> and Hee-Je Kim <sup>1,\*</sup>

<sup>1</sup> School of Electrical Engineering, Pusan National University, Busandaehak-ro 63beongil, Geumjeong-gu, Busan 46241, Korea; kanakadurga.ikkurthi@gmail.com (I.K.D.); cyon67@hanmail.net (T.-Y.P.); imjsn17@pusan.ac.kr (B.J.-S.); whdlsgh92@icloud.com (C.-I.H.); kprabakar@gmail.com (K.P.)

<sup>2</sup> Department of Mechatronics Engineering, KyungSung University, 309 Suyeong-ro Nam-gu, Busan 48434, Korea; srinu.krs@gmail.com (S.S.R.); jwahn@ks.ac.kr (J.-W.A.)

\* Correspondence: heeje@pusan.ac.kr; Tel.: +82-51-510-2364; Fax: +82-51-513-0212

Received: 13 June 2018; Accepted: 19 June 2018; Published: 21 June 2018



**Abstract:** A cost-effective and uniform crystal with different structures was fabricated using a facile chemical bath deposition technique for electrochemical supercapacitor (SC) applications. In this study, CuS, PbS, and CuS@PbS composite electrodes were fabricated for SCs. The morphology and structure of the electrodes were analyzed by field emission–scanning electron microscopy, transmission electron microscopy, X-ray diffraction, and X-ray photoelectron spectroscopy. The CuS@PbS composite electrode delivered outstanding electrochemical performance in SCs with a high specific capacitance of 1004.42 F g<sup>-1</sup> at a current density of 2.85 A g<sup>-1</sup>, good cycling stability (only 2.9% loss after 3000 cycles at 2.85 A g<sup>-1</sup>), higher energy density of 33.89 Wh kg<sup>-1</sup> at a power density of 714.28 W kg<sup>-1</sup>, and an excellent rate capability compared to other electrodes. These results show that the CuS@PbS composite can be used to improve the surface morphology and is a promising positive electrode material for SC applications.

**Keywords:** supercapacitors; CuS@PbS composite; chemical bath deposition; cyclic voltammetry

## 1. Introduction

Environmentally friendly, efficient, and sustainable energy resources are attracting increasing attention in the modern electronics industry. Supercapacitors (SCs) have received tremendous interest owing to their light weight, high performance, stability, low maintenance cost, safer operation, and environmental friendliness [1,2]. SCs exhibit a higher power density than Li-ion batteries, which depend on the properties and structure of the materials [3]. SCs can be classified into two categories based on the charge storage mechanism: electrochemical double layer capacitors (EDLCs) and pseudocapacitors. EDLCs store electrical energy by the separation of charge at the interface between the electrode/electrolyte, and pseudocapacitors exploit reversible faradaic redox reactions near the electrode surface.

According to the charge storage mechanism, pseudocapacitors have a much higher energy density and specific capacitance than EDLCs. Pseudocapacitor materials, such as conducting polymers/metal oxides, are used for high performance because of their low cost, low toxicity, good flexibility, and appropriate morphology [4–6]. Transition metal sulfides, such as CoS, NiS, ZnS, SnS, and CuS, are attractive electrode materials for SCs because of their superior capacitive performance, natural abundance, and low cost [7–12]. In particular, the environmental friendliness of CuS makes it a promising candidate for SC applications [13,14]. In the past, CuS has been used as a counter electrode for

photoelectrochemical cells because of its redox reaction with the poly sulfide electrode, sometimes, CuS has been used as a cathode material for recharge batteries. Moreover, CuS has been used as an electrode material for lithium ion batteries because of its high energy capacity and good electronic conductivity.

Zhu et al. prepared CuS nanoneedles on a CNT backbone with hierarchical nanostructures (CNT@CuS) as a SC electrode material that exhibited a high capacitance of  $122 \text{ F g}^{-1}$  with excellent cycling stability [15]. Hsu et al. Prepared CuS nanowire arrays fabricated on Cu foil with a high specific capacitance of  $305 \text{ F g}^{-1}$  [16]. Peng et al. reported CuS with hierarchical structures with a maximum specific capacitance of  $597 \text{ F g}^{-1}$  at  $1 \text{ A g}^{-1}$  [17].

PbS belongs to the metal sulfide family with a narrow band gap of 0.41 eV, high absorption coefficient of  $1\text{--}5 \times 10^5 \text{ cm}^{-1}$  and a large Bohr exciton radius of 18 nm [18,19]. A power conversion efficiency of 10% was achieved for PbS quantum dots-based depleted heterojunction solar cells [20]. To the best of the authors' knowledge, there are few reports of composite materials of a conductive polymer and a hierarchical copper sulfide for SC applications. Moreover, there is little information on the synthesis of PbS materials as an electrode for high performance SCs.

The performance of SC materials depends multiple parameters, such as the surface morphology, adhesion on the substrate, reaction temperature and time, and nanostructure properties. On the other hand, the surface morphology and nanostructures of the active electrodes are affected by their particle size distribution, surface area, and material thickness. These parameters play a key role that determine the active sites for electrochemical reactions and kinetics of the SC electrodes, transport/diffusion paths, and accessibility of redox electrolyte [21–24].

In this study, a cost effective, facile strategy was developed for the design and fabrication of a CuS@PbS composite on a nickel foam substrate using a chemical bath deposition (CBD) method for SC applications. The deposition time and temperature were optimized for CuS@PbS composite electrodes, which were characterized by electrochemical impedance spectroscopy (EIS), cyclic voltammetry (CV), and galvanostatic charge-discharge (GCD) tests in a 3 M KOH solution. The electrode materials delivered a high specific capacitance of  $1004.22 \text{ F g}^{-1}$  at  $2.85 \text{ A g}^{-1}$ , energy density of  $33.89 \text{ Wh kg}^{-1}$  at a power density of  $714.28 \text{ W kg}^{-1}$ , and approximately 97.1% capacity retention after 3000 cycles. These results highlight the potential of CuS@PbS composite as a long-term performance electrode material for SC applications.

## 2. Experimental Methods

### 2.1. Materials

All chemicals, such as copper sulfate [ $\text{CuSO}_4$ ], lead (II) nitrate [ $\text{Pb}(\text{NO}_3)_2$ ], urea [ $\text{CH}_4\text{N}_2\text{O}$ ], thioacetamide [ $\text{C}_2\text{H}_5\text{NS}$ ], and nickel (Ni) foam, were purchased from Sigma Aldrich and used as received.

### 2.2. Synthesis of CuS, PbS and CuS@PbS Electrodes

Prior to fabrication, a piece of Ni foam was cut into  $1 \times 1 \text{ cm}^2$  and the substrate was cleaned by sonication in acetone, ethanol, and DI water for 20 min each. For the synthesis of the CuS@PbS electrode, 1.11 g of  $\text{CuSO}_4$ , 1.68 g of  $\text{CH}_4\text{N}_2\text{O}$ , 2.31 g of  $\text{Pb}(\text{NO}_3)_2$ , and 2.10 g of  $\text{C}_2\text{H}_5\text{NS}$ , were dissolved in 70 ml of DI water with vigorous stirring for 30 min to form a homogeneous solution. After stirring for 30 min, the solution was transferred to a flask and the well-cleaned nickel foam substrates were dropped vertically in the resulting solution and kept in a hot air oven at  $90 \text{ }^\circ\text{C}$  for 3 h. The resulting electrodes were washed several times with ethanol and distilled water and dried in a vacuum oven at  $60 \text{ }^\circ\text{C}$  for 2 h. CuS and PbS electrodes were also prepared using the same procedure without lead and/or copper sources and used for further characterization.

### 2.3. Materials Characterization

The surface morphology and structure of the films was analyzed by field emission scanning electron microscopy (FE-SEM, S-2400, Hitachi, Tokyo, Japan) and transmission electron microscopy

(TEM, Tecnai G2 F20, Tokyo, Japan). The crystallinity and phase purity of the as-prepared electrode were analyzed by X-ray diffraction (XRD, D/Max-2400, Rigaku, Tokyo, Japan) using a Cu  $\alpha$  source over the  $2\theta$  range of  $20\text{--}80^\circ$ . The chemical states of the elements were examined by X-ray photoelectron spectroscopy (XPS, KBSI, Busan, Korea).

#### 2.4. Electrochemical Measurements

The electrochemical measurements were conducted in a three-electrode system. CuS, PbS, and CuS@PbS were used as the working electrode; Ag/AgCl as the reference electrode; and Pt wire used as the counter electrode. In this study, we used 3 M KOH aqueous solution for electrochemical measurements due to its multiple advantages: (1)  $\text{K}^+$  has the highest ionic conductivity after  $\text{H}_3\text{O}^+$  among cations and  $\text{OH}^-$  has the highest ionic conductivity among anions; (2) the price of KOH is much cheaper than that of non-aqueous organic ones or ionic liquids; and (3) assembling procedure of supercapacitors with water-based solutions is very easy. The weight of the active material was almost  $7\text{--}9\text{ mg cm}^{-2}$  for all electrodes. Electrochemical measurements including CV, GCD, and EIS were measured using a Biologic-SP150 workstation. CV was conducted at various scan rates (10, 20, 30, 40, and  $50\text{ mV s}^{-1}$ ) between 0.1 to  $-0.6\text{ V}$  vs. Ag/AgCl. The GCD test was conducted between  $-0.1$  to  $0.4\text{ V}$  with different current densities to calculate the specific capacitance. EIS was conducted over the frequency range, 100 kHz to 0.1 Hz. The power ( $P$ ) and energy ( $E$ ) densities of the electrodes were estimated from the GCD curves using the following equations [25,26]:

$$C_s = \frac{i \times \Delta t}{m \times \Delta V} \quad (1)$$

$$E = \frac{1}{2C_s(\Delta V)^2} \times \frac{1000}{3600} \quad (2)$$

$$P = \frac{E}{t} = \frac{i\Delta V}{2m} \times 1000 \quad (3)$$

where  $C_s$  is the specific capacitance;  $I$  is the discharge current;  $t$  is the discharge time;  $V$  is the voltage window between the positive and negative electrodes; and  $m$  is the mass of the active material.

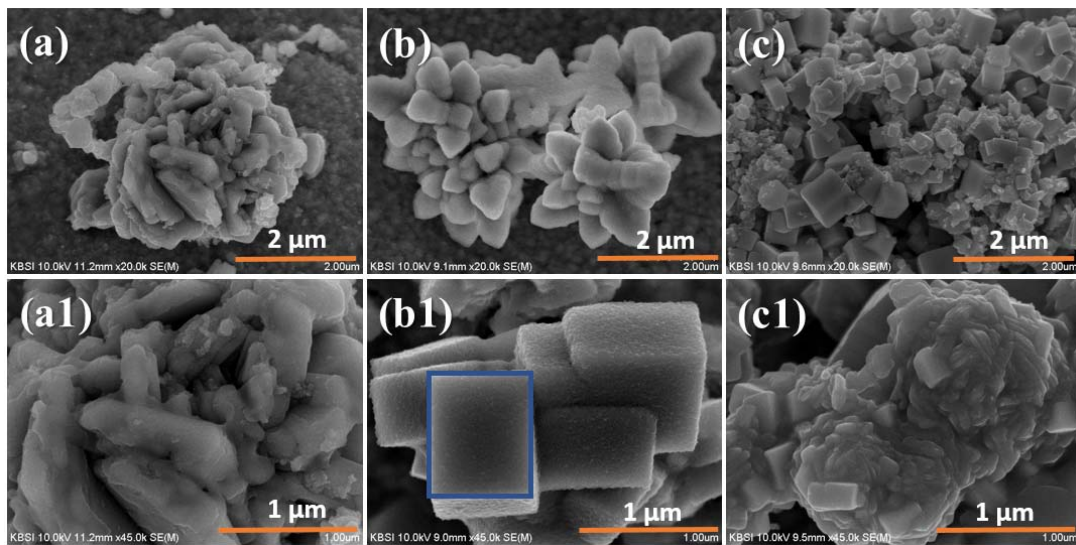
### 3. Results and Discussion

Figure 1 shows high and low magnification FE-SEM images of the surface morphology and structure of the CuS, PbS, and CuS@PbS composite electrodes on nickel foam substrates. Figure 1(a,a1) presents FE-SEM images of the CuS electrode, which shows a crystal structure with uniform deposition. Figure 1b shows that the PbS electrodes consists of a jasmine flower structure and is composed of many nano-sheets and flower-like structures with a large surface area deposited on nickel foam and shows a rectangular sugar cube structure. As shown in Figure 1(c,c1), the CuS and PbS dice were dispersed uniformly and the presence of CuS inhibited the close stacking of PbS, which can enlarge the spaces and leading microstructures. Figure 1c shows that the CuS particles on the surface of the PbS dice sheets can prevent the aggregation of particles and enhance the surface area of the material. In Figure 2(c,c1), the dice-like nanostructure could be observed clearly in the composite.

Figure 2d–j shows the energy dispersive X-ray spectroscopy (EDX, S-2400, Hitachi, Tokyo, Japan) data of CuS, PbS, and CuS@PbS composite electrodes. EDX showed that the CuS, PbS, and CuS@PbS were composed of Cu and S; Pb and S; and Cu, Pb, and S in the atomic percentage of 42.80%, 57.20% for CuS; 58.57% and 41.43% for PbS; and 68.20%, 0.16%, and 31.64% for the composite; respectively. These results show that the materials had been deposited successfully on the surface of the nickel form.

The crystallinity and phase purity of the as-prepared samples were characterized by X-ray diffraction on nickel foam substrates, as shown in Figure 3. In the XRD pattern, the nickel foam substrate showed three strong peaks at  $44.5^\circ$ ,  $51.8^\circ$ , and  $76.4^\circ$   $2\theta$ . The XRD peaks for CuS were observed at  $29.3^\circ$ ,  $32.8^\circ$ ,  $52.7^\circ$ , and  $59.4^\circ$   $2\theta$ . All peaks for CuS were well matched with the Joint

Committee for Powder Diffraction Studies (JCPDS card no. 06-0464), and the PbS peaks shown at  $70.9^\circ$  and  $78.8^\circ$   $2\theta$  matched the JCPDS card no. 05-0592.



**Figure 1.** (a–c) Low and high (a1–c1) resolution FE-SEM images of the prepared CuS, PbS and CuS@PbS composite.

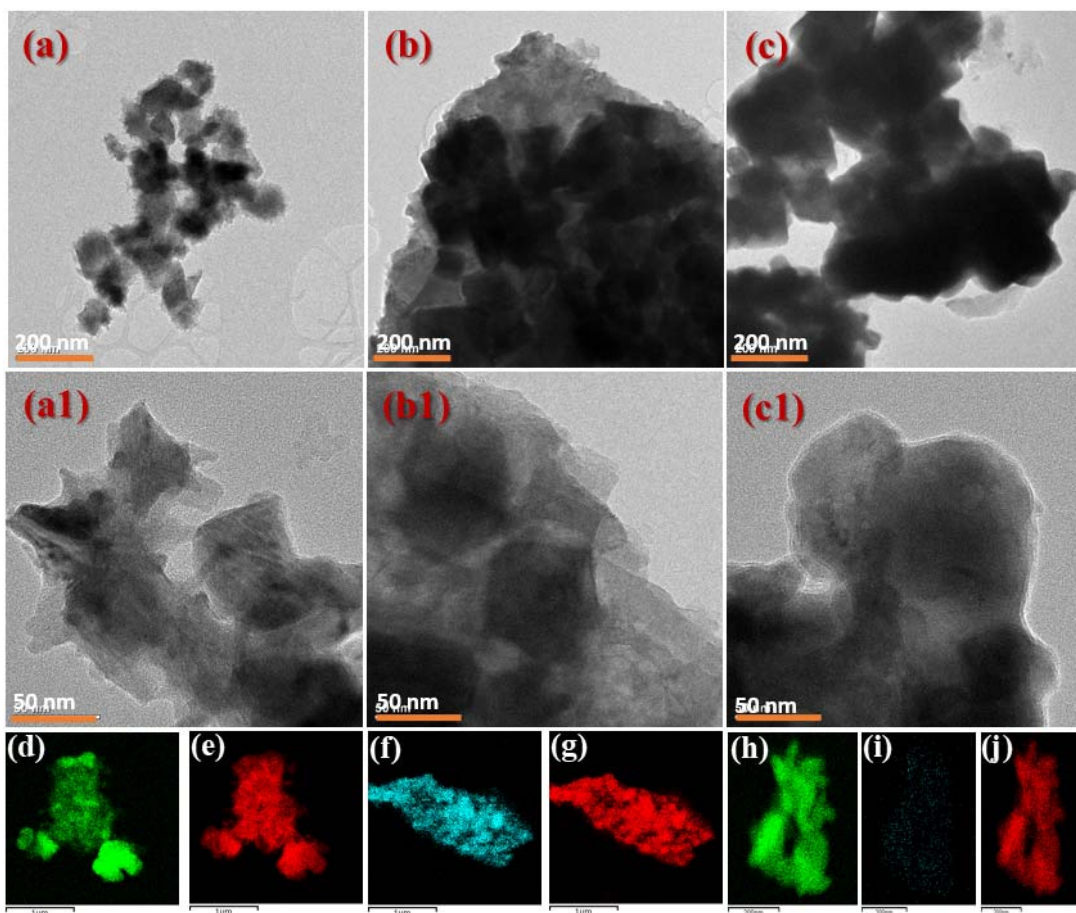


**Figure 2.** Low magnification (a–c) and high-magnification (a1–c1) TEM images of CuS (a,a1), PbS (b,b1) and CuS@PbS (c,c1) composite on Ni-foam substrate. EDX-TEM image and corresponding elemental mapping of CuS (d,e), PbS (f,g) and composite (h–j).

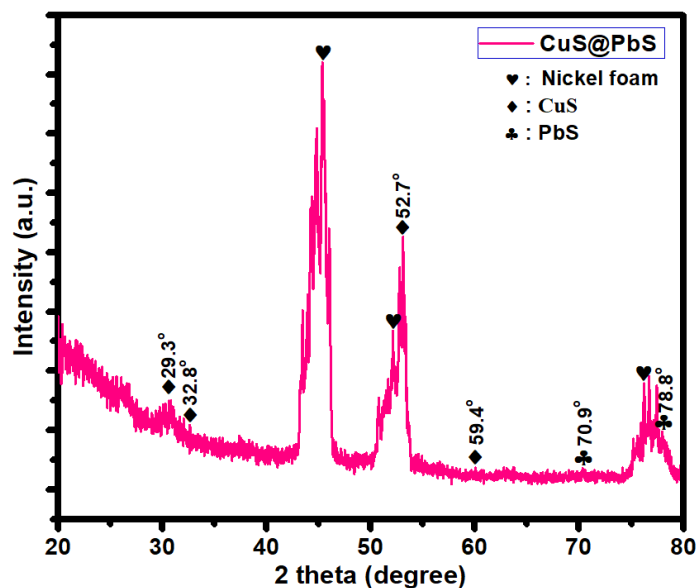


Figure 3. X-ray diffraction pattern of the prepared CuS@PbS composite.

XPS was performed to determine the chemical composition of the prepared materials. Figure 4a presents the survey spectrum of the CuS, PbS, and CuS@PbS composite. The spectrum revealed Cu, Ni, O, C, and S for CuS; Ni, O, C, S, and Pb for PbS; and Cu, Pb, S, Ni, C, and O for the CuS@PbS composite. Figure 4b shows the high resolution Cu2p peaks at 934.0 eV for Cu2p<sub>3/2</sub> and 953.87 eV for Cu2p<sub>1/2</sub> [27,28]. The difference in binding energy of these two peaks was approximately 19.87 eV. Figure 4c shows Pb4f peaks at 137.5 eV for Pb4f<sub>1/2</sub> and 142.4 eV for Pb4f<sub>3/2</sub>; the binding energy of the two peaks was 4.9 eV [29]. The peaks at 162.70 and 168.23 eV in the high-resolution XP spectrum (Figure 4d) were assigned to S2p, which shows that the composite had been synthesized successfully, which is good agreement with the XRD pattern.

As a novel electrode material, the PbS-anchored CuS sample was used in SC applications and the results were compared with those of the bare CuS and PbS electrodes. CV was conducted at a scanning rate of 10 mV s<sup>-1</sup> in a 3 M KOH solution. As shown in Figure 5a, the CuS@PbS composite showed the largest area in the CV plot compared to the bare CuS and PbS electrodes, indicating higher specific capacitance [30]. The rate capability and reversibility of CuS, PbS, and CuS@PbS were examined further by CV and galvanostatic charge-discharge (GCD) analysis at various scan rates and current densities. With increasing scan rates from 10 to 50 mV s<sup>-1</sup> (Figure 5d), the composite displayed higher oxidation and lower reduction currents. Moreover, the anodic and cathodic peaks shifted to a more positive and negative voltage, which was caused by the sluggish rate of electronic and ionic transport and the kinetics of the interfacial reaction [31].

GCD was conducted to evaluate the electrochemical capacitance of CuS, PbS, and CuS@PbS electrodes. GCD was performed in different current densities of 2.85, 4.28, 5.71 and 7.14 A g<sup>-1</sup> in 3 M KOH over the potential range of -0.1 to 0.4 V (Figure 6). From eq. (1), the specific capacitance of the CuS@PbS composite was 1004.22, 905.91, 823.65, 752.14, 678.68, 628.6, 583.77, 536.4, and 502.0 F g<sup>-1</sup> at a current density of 2.85, 4.28, 5.71, 7.14, 8.57, 10.0, 11.42, 12.85, and 14.28 A g<sup>-1</sup>, respectively. The specific capacitances of the CuS and PbS electrodes were also calculated at the same current densities as the CuS@PbS composite: 326.22, 288.42, 257.6, 227.57, 194.22, 166.4, 147.65, 130.88, and 117.71 F g<sup>-1</sup>, respectively; and 228.28, 186.25, 148.45, 118.42, 94.45, 73.6, 56.68, 41.4, and 27.14 F g<sup>-1</sup>, respectively. The specific capacitance decreased gradually with increasing current density from 2.85 to 14.28 A g<sup>-1</sup> due to the resistance of the electrode and insufficient faradaic redox reaction at high current densities (Figure 6d) [32]. When the current density was increased to 14 A g<sup>-1</sup> for the composite, the specific capacitance reached 500 F g<sup>-1</sup>, demonstrating superior electrochemical performance to individual

CuS and PbS. The CuS@PbS composite electrode showed a high specific capacitance of  $1004.22 \text{ F g}^{-1}$  at  $2.85 \text{ A g}^{-1}$ , which was higher than CuS ( $326.22 \text{ F g}^{-1}$ ) and PbS ( $228.28 \text{ F g}^{-1}$ ). The higher specific capacitance was attributed to its higher surface area with the improved surface morphology of nanostructures. The main reasons for the higher specific capacitance of the composite is (1) great adhesion and higher surface area which can offer extra electron transport pathways and more active sites for Faradaic redox reactions. The higher electrochemical properties observed is mainly due to the synergistic effect and improved surface morphology of nanostructure which can provides a numerous fast electron-transport access to the current collector. Importantly, CuS and PbS are the promising electrode material for the SCs due to being environmentally friendly, low-cost and earth-abundant. To the best of author's knowledge, the CuS@PbS composite exhibited highest values compared to many published reports (See Table 1).

**Table 1.** Comparison of specific capacitance of CuS@PbS composite with different electrodes.

Material	Electrolyte	Current Density	Specific Capacitance	Ref.
CuS@PbS composite	3 M KOH	$2.85 \text{ A g}^{-1}$	$1004.42 \text{ F g}^{-1}$	This study
NiS nanoparticles	2 M KOH	$0.5 \text{ A g}^{-1}$	$516 \text{ F g}^{-1}$	[33]
rGO-NiS	-	$2.5 \text{ A g}^{-1}$	$109.37 \text{ F g}^{-1}$	[34]
$\text{Co}_3\text{O}_4$ @Pt@MnO <sub>2</sub> NA	1.0 M Na <sub>2</sub> SO <sub>4</sub>	$1 \text{ A g}^{-1}$	$539 \text{ F g}^{-1}$	[35]
CuS@PANI	0.1 M Li <sub>2</sub> SO <sub>4</sub>	$0.5 \text{ A g}^{-1}$	$308.1 \text{ F g}^{-1}$	[36]
Graphene/NiCo <sub>2</sub> S <sub>4</sub> /Co <sub>x</sub> Ni <sub>(3-x)</sub> S <sub>2</sub>	-	$10 \text{ mA cm}^{-2}$	$15.6 \text{ F/cm}^2$	[37]
CoS-NP/CoS-NS DSNB	2 M KOH	$1 \text{ A g}^{-1}$	$980 \text{ F g}^{-1}$	[38]
ZnS/G-60	6 M KOH	$5 \text{ mV s}^{-1}$	$197.1 \text{ F g}^{-1}$	[9]
FL-SnS <sub>2</sub>	2 M KOH	$1 \text{ A g}^{-1}$	$431.82 \text{ F g}^{-1}$	[39]

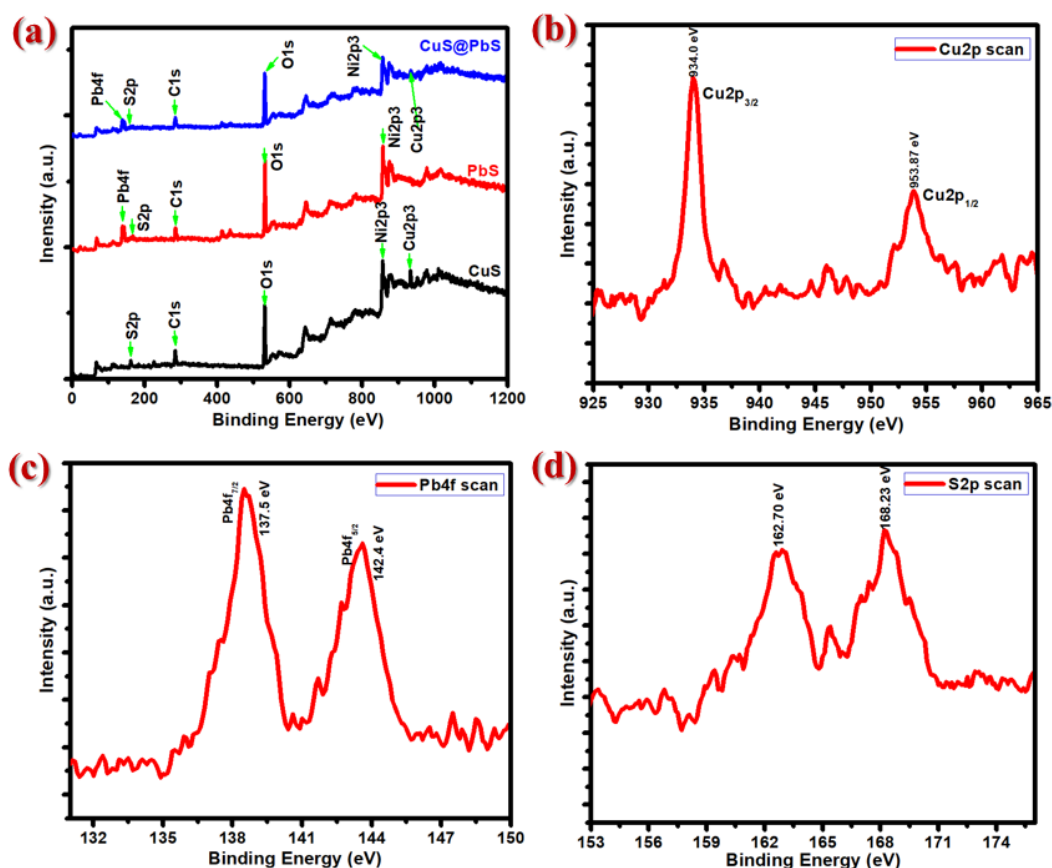


**Figure 4.** (a) XPS survey spectrum of CuS, PbS and CuS@PbS composite. (b) Cu2p scan, (c) Pb4f scan and (d) S2p core level spectra of CuS@PbS composite.

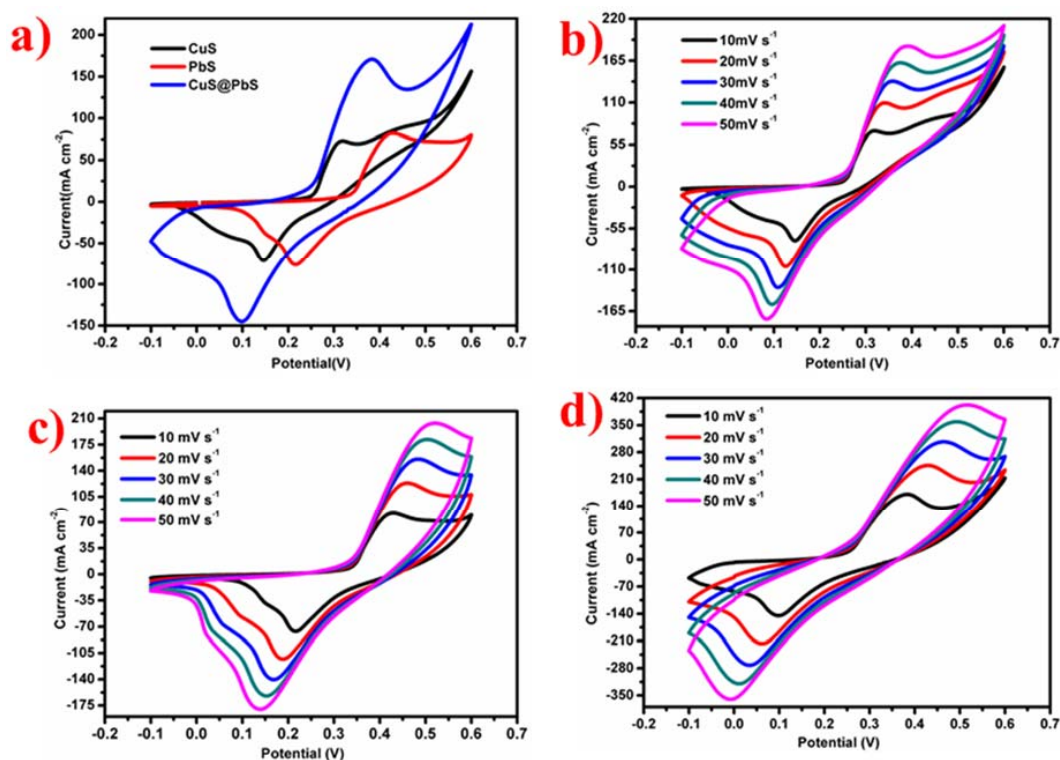


**Figure 5.** (a) Comparison CV curves of the CuS, PbS and CuS@PbS electrodes at the scan rate of  $10 \text{ mV s}^{-1}$ . CV curves of the (b) CuS, (c) PbS, (d) CuS@PbS electrodes at different scan rates of  $10\text{--}50 \text{ mV s}^{-1}$  in  $3 \text{ M KOH}$  solution.

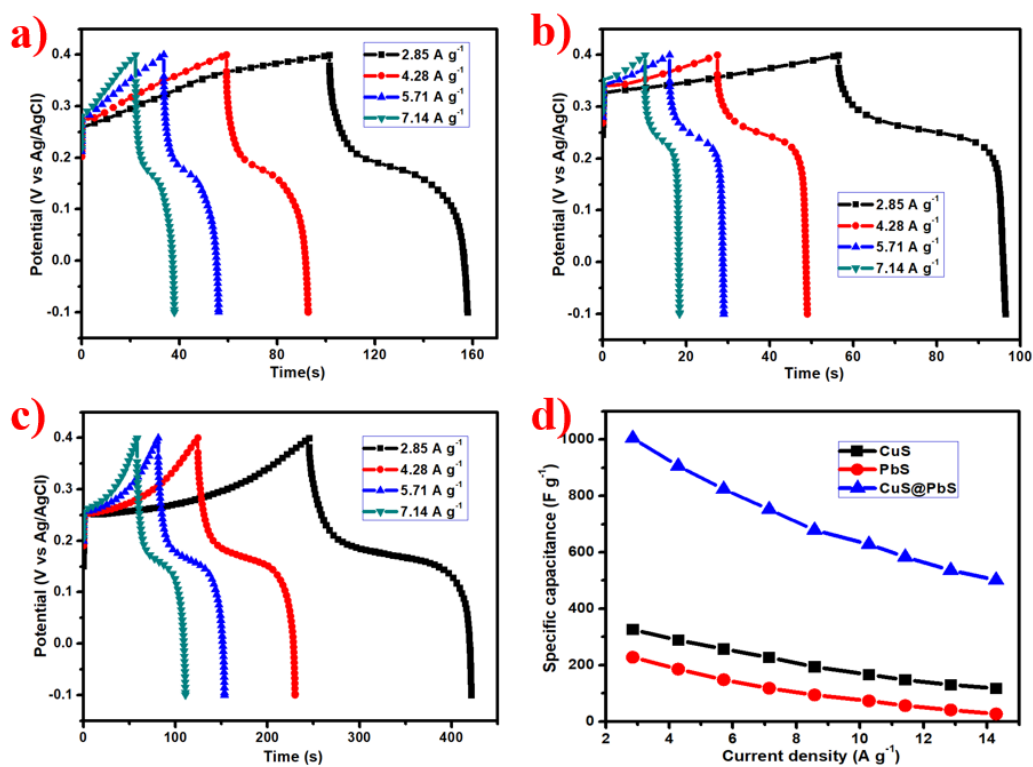


**Figure 6.** Charge and discharge curves of the (a) CuS, (b) PbS and (c) CuS@PbS composite electrodes at different current densities of  $2.85, 4.28, 5.71$  and  $7.14 \text{ A g}^{-1}$  in  $3 \text{ M KOH}$  solution; (d) specific capacitance as a function of current density.

EIS was used to study the resistive and capacitive behavior over the frequency range of 0.01 Hz to 100 kHz at the open-circuit potential with an amplitude of 5 mV. The Nyquist impedance plots in Figure 7 show a semi-circle at high frequency and a steep linear curve at the low-frequency region. At high frequencies, the series resistance ( $R_s$ ) and charge-transfer resistance ( $R_{ct}$ ) can be evaluated from the intercepts of the high-frequency semicircle on the  $Z'$ -axis. According to the curves, the  $R_s$  value of the CuS@PbS electrode was lower than that of the other two electrodes (CuS, PbS), which reflects the good electrical conductivity and easy charge-transfer kinetics in the CuS@PbS electrode. The composite exhibited low  $R_s$  and  $R_{ct}$  values, which indicates that the contact resistance and charge transfer resistance in the CuS@PbS are low. The straight vertical line in the inset shows the pure capacitive nature of CuS, PbS, and CuS@PbS, which is related to ion diffusion in the electrode and the diffusion resistance of the KOH electrolyte into the interior of the electrode [25,26].

A Ragone plot is used to identify the energy and power density of CuS, PbS, and CuS@PbS (Figure 8). The energy and power density were calculated using the GCD data, according to Equations (2) and (3) in the experimental section. CuS@PbS showed a good energy density of  $33.89 \text{ Wh kg}^{-1}$  at a power density of  $714.28 \text{ W kg}^{-1}$ , which were much higher than the CuS ( $11.01 \text{ Wh kg}^{-1}$ ) and PbS ( $7.70 \text{ Wh kg}^{-1}$ ) electrodes.

The cycling performance of the CuS, PbS, and CuS@PbS composite electrode were measured at a current density of  $2.85 \text{ A g}^{-1}$ . As shown in Figure 9, the specific capacitance of the CuS@PbS composite decreased slowly from  $1004.22 \text{ F g}^{-1}$  to  $975.09 \text{ F g}^{-1}$  after 3000 cycles; CuS decreased from  $326.22 \text{ F g}^{-1}$  to  $297.51 \text{ F g}^{-1}$  and PbS decreased from  $228.28 \text{ F g}^{-1}$  to  $204.33 \text{ F g}^{-1}$ . Moreover, the specific capacitance of the CuS@PbS composite electrode lost only 2.9% (approximately 97.1% capacity retention), whereas the CuS and PbS electrodes lost 8.8% and 10.49%, respectively, after 3000 cycles. These results highlight the good long-term cycling stability of the CuS@PbS composite electrode. The high performance, greater long-term stability of the CuS@PbS electrode suggests that low-cost PbS anchored with the MnS electrode has considerable application potential in energy storage.

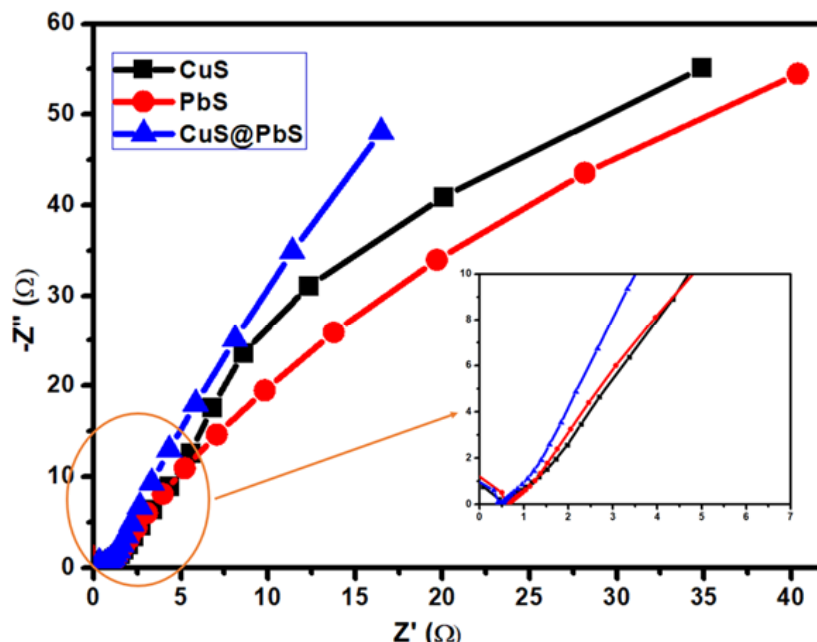


Figure 7. Impedance Nyquist plots of the CuS, PbS and CuS@PbS electrodes.

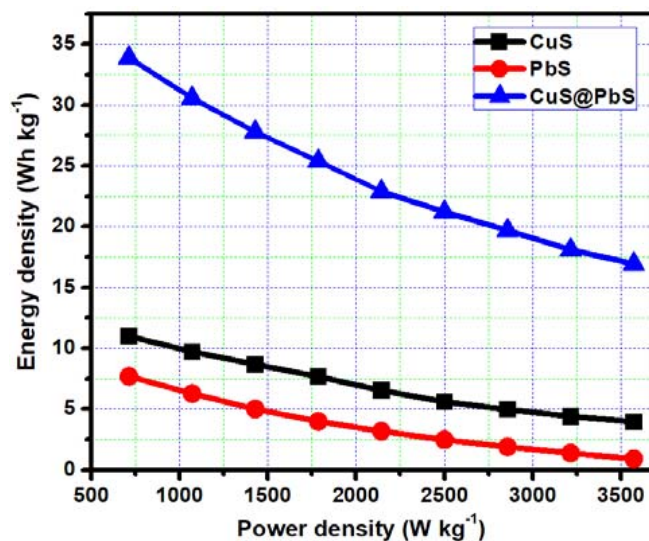


Figure 8. Ragone plots of the CuS, PbS and CuS@PbS-based electrodes.

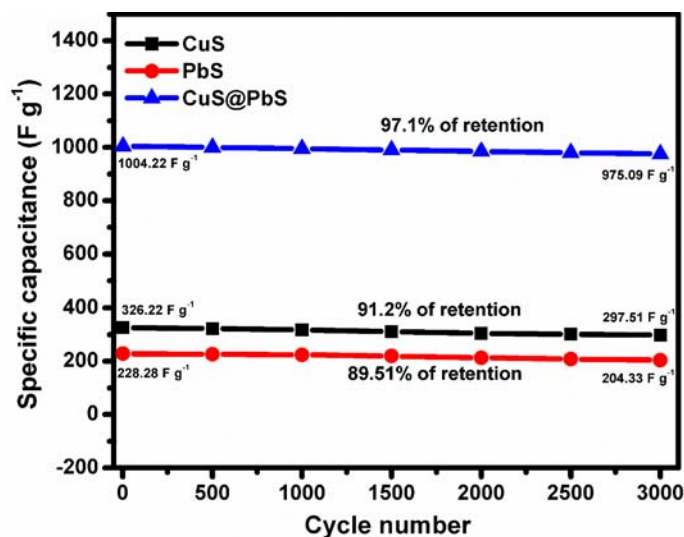


Figure 9. Life cycle of CuS, PbS and CuS@PbS composite electrodes in KOH solution at current density of  $2.85 \text{ A g}^{-1}$  for 3000 cycles.

#### 4. Conclusions

In this study, a dice-like CuS@PbS nanostructure was synthesized using a facile chemical bath deposition method. The dice-like nanostructure provided suitable ionic transportation channels, higher surface area, rapid electronic conductive pathways, and more active sites for the electrochemical reaction. As the electrochemical results showed that at charge and discharge at a current density of  $2.85 \text{ A g}^{-1}$ , the initial specific capacitance of CuS@PbS ( $1004.22 \text{ F g}^{-1}$ ) was approximately 3.07 and 4.39 times higher, respectively, than that of CuS ( $326.22 \text{ F g}^{-1}$ ) and PbS ( $228.28 \text{ F g}^{-1}$ ). The CuS@PbS electrode has superior cycling stability over 3000 cycles and shows 97.1% retention, which is higher than that of CuS (91.2%) and PbS (89.51%). The present study shows that the PbS anchored with CuS generates large electrode/electrolyte interfaces and is a promising active material for cost-effective, large-scale, and electrochemically stable SCs.

**Author Contributions:** I.K.D., S.S.R. and T.-Y.P. conceived and designed the experiments; I.K.D. and B.J.-S. Performed the experiments; C.I.H. and K.P. analyzed the data; H.-J.K. contributed reagents/materials/analysis tools; J.-W.A. and I.K.D. answered all review questions; I.K.D. wrote the paper.

**Funding:** This research received no external funding.

**Acknowledgments:** This research was supported by Basic Research Laboratory through the National Research Foundations of Korea funded by the Ministry of Science, ICT and Future Planning (NRF-2015R1A4A1041584). We also thankful to KBSI for HR-SEM, TEM, XRD and XPS measurements.

**Conflicts of Interest:** The authors declare no conflict of interest.

## References

1. Simon, P.; Gogotsi, Y. Materials for electrochemical capacitors. *Nat. Mater.* **2008**, *7*, 845–854. [[CrossRef](#)] [[PubMed](#)]
2. Meng, C.; Liu, C.; Chen, L.; Hu, C.; Fan, S. Highly Flexible and All-Solid-State Paper like Polymer Supercapacitors. *Nano Lett.* **2010**, *10*, 4025–4031. [[CrossRef](#)] [[PubMed](#)]
3. Liu, B.; Wang, X.F.; Chen, H.T.; Wang, Z.R.; Chen, D.; Cheng, Y.B.; Zhou, C.W.; Shen, G.Z. Hierarchical silicon nanowires-carbon textiles matrix as a binder-free anode for high-performance advanced lithium-ion batteries. *Sci. Rep.* **2013**, *3*, 1622–1627. [[CrossRef](#)] [[PubMed](#)]
4. Ramkumar, R.; Manickam, M.S. Electrochemical synthesis of polyaniline cross-linked NiMoO<sub>4</sub> nanofibre dendrites for energy storage devices. *New J. Chem.* **2016**, *40*, 7456–7464. [[CrossRef](#)]
5. Maryam, J.B.; Manickam, M. Tuning the Redox Properties of the Nanostructured CoMoO<sub>4</sub> Electrode: Effects of Surfactant Content and Synthesis Temperature. *ChemPlusChem* **2016**, *81*, 964–977.
6. Rashmirekha, S.; Barsha, D.; Chinmaya, K.S.; Kali, S.; Tondepu, S.; Gamini, S.; Manickam, M. Influence of Synthesis Temperature on the Growth and Surface Morphology of Co<sub>3</sub>O<sub>4</sub> Nanocubes for Supercapacitor Applications. *Nanomaterials* **2017**, *7*, 356.
7. Jiang, Z.; Lu, W.; Li, Z.; Ho, K.H.; Li, X.; Jiao, X.; Chen, J.D. Synthesis of amorphous cobalt sulfide polyhedral nanocages for high performance supercapacitors. *Mater. Chem. A* **2014**, *2*, 8603–8606. [[CrossRef](#)]
8. Wei, C.; Cheng, C.; Zhao, J.; Wang, Y.; Cheng, Y.; Xu, Y.; Du, W.; Pang, H. NiS Hollow Spheres for High-Performance Supercapacitors and Non-Enzymatic Glucose Sensors. *Chem. Asian J.* **2015**, *10*, 679–686. [[CrossRef](#)] [[PubMed](#)]
9. Ramachandran, R.; Saranya, M.; Kollu, P.; Raghupathy, B.P.C.; Jeong, S.K.; Grace, A.N. Solvothermal synthesis of Zinc sulfide decorated Graphene (ZnS/G) nanocomposites for novel Supercapacitor electrodes. *Electrochim. Acta* **2015**, *178*, 647–657. [[CrossRef](#)]
10. Chauhan, H.; Singh, M.K.; Hashmi, S.A.; Deka, S. Synthesis of surfactant-free SnS nanorods by a solvothermal route with better electrochemical properties towards supercapacitor applications. *RSC Adv.* **2015**, *5*, 17228–17235. [[CrossRef](#)]
11. Justin Raj, C.; Kim, B.C.; Cho, W.-J.; Lee, W.-G.; Seo, Y.; Yu, K.-H. Electrochemical capacitor behavior of copper sulfide (CuS) nanoplatelets. *J. Alloy. Compd.* **2014**, *586*, 191–196. [[CrossRef](#)]
12. Huang, K.-J.; Zhang, J.-Z.; Ia, Y.-L.; Xing, K.; Liu, Y.-M. Acetylene black incorporated layered copper sulfide nanosheets for high-performance supercapacitor. *J. Alloy. Compd.* **2015**, *641*, 119–126. [[CrossRef](#)]
13. Huang, K.-J.; Zhang, J.-Z.; Liu, Y.; Liu, Y.-M. Synthesis of reduced graphene oxide wrapped-copper sulfide hollow spheres as electrode material for supercapacitor. *J. Hydrogen Energy* **2015**, *40*, 10158–10167. [[CrossRef](#)]
14. Zhang, G.Q.; Lou, X.W. General Solution Growth of Mesoporous NiCo<sub>2</sub>O<sub>4</sub> Nanosheets on Various Conductive Substrates as High-Performance Electrodes for Supercapacitors. *Adv. Mater.* **2013**, *25*, 976–979. [[CrossRef](#)] [[PubMed](#)]
15. Zhu, T.; Xia, B.; Zhou, L.; Lou, X. Arrays of ultrafine CuS nanoneedles supported on a CNT backbone for application in supercapacitors. *J. Mater. Chem.* **2012**, *22*, 7851–7855. [[CrossRef](#)]
16. Hsu, Y.-K.; Chen, Y.-C.; Lin, Y.-G. Synthesis of copper sulfide nanowire arrays for high-performance supercapacitors. *Electrochim. Acta* **2014**, *139*, 401–407. [[CrossRef](#)]
17. Peng, H.; Ma, G.; Mu, J.; Sun, K.; Lei, Z. Controllable synthesis of CuS with hierarchical structures via a surfactant-free method for high-performance supercapacitors. *Mater. Lett.* **2014**, *122*, 25–28. [[CrossRef](#)]
18. Tian, J.; Shen, T.; Liu, X.; Fei, C.; Lv, L.; Cao, G. Enhanced Performance of PbS-quantum-dot-sensitized Solar Cells via Optimizing Precursor Solution and Electrolytes. *Sci. Rep.* **2016**, *6*, 23094. [[CrossRef](#)] [[PubMed](#)]
19. Jiao, S.; Wang, J.; Shen, Q.; Li, Y.; Zhong, X. Surface engineering of PbS quantum dot sensitized solar cells with a conversion efficiency exceeding 7%. *J. Mater. Chem. A* **2016**, *4*, 7214–7221. [[CrossRef](#)]

20. Kim, G.H.; García de Arquer, F.P.; Yoon, Y.J.; Lan, X.; Liu, M.; Voznyy, O.; Jagadamma, L.K.; Abbas, A.S.; Yang, Z.; Fan, F.; et al. High-Efficiency Colloidal Quantum Dot Photovoltaics via Robust Self-Assembled Monolayers. *Nano Lett.* **2015**, *15*, 7691–7696. [[CrossRef](#)] [[PubMed](#)]
21. Yu, Z.; Tetard, L.; Zhai, L.; Thomas, J. Supercapacitor electrode materials: Nanostructures from 0 to 3 dimensions. *Energy Environ. Sci.* **2015**, *8*, 702–730. [[CrossRef](#)]
22. Xu, J.; Wang, X.; Wang, X.; Chen, D.; Chen, X.; Li, D.; Shen, G. Three-Dimensional Structural Engineering for Energy-Storage Devices: From Microscope to Macroscopic. *ChemElectroChem* **2014**, *1*, 975–1002. [[CrossRef](#)]
23. Moosavifard, S.E.; El-Kady, M.F.; Rahmanifar, M.S.; Kaner, R.B.; Mousavi, M.F. Designing 3D Highly Ordered Nanoporous CuO Electrodes for High-Performance Asymmetric Supercapacitors. *ACS Appl. Mater. Interfaces* **2015**, *7*, 4851–4860. [[CrossRef](#)] [[PubMed](#)]
24. Buller, S.; Strunk, J. Nanostructure in energy conversion. *J. Energy Chem.* **2016**, *25*, 171–190. [[CrossRef](#)]
25. Rao, S.S.; Durga, I.K.; Kundakarla, N.; Punnoose, D.; Gopi, C.V.V.M.; Reddy, A.E.; Jagadeesh, M.; Kim, H.J. A hydrothermal reaction combined with a post anion-exchange reaction of hierarchically nanostructured NiCo<sub>2</sub>S<sub>4</sub> for high-performance QDSSCs and supercapacitors. *New J. Chem.* **2017**, *41*, 10037–10047. [[CrossRef](#)]
26. Rao, S.S.; Punnoose, D.; Bae, J.H.; Durga, I.K.; Varma, C.V.T.; Naresh, B.; Subramanian, A.; Raman, V.; Kim, H.J. Preparation and electrochemical performances of NiS with PEDOT:PSS chrysanthemum petal like nanostructure for high performance supercapacitors. *Electrochim. Acta* **2017**, *254*, 269–279.
27. Durga, I.K.; Rao, S.S.; Reddy, A.E.; Gopi, C.V.V.M.; Kim, H.J. Achieving copper sulfide leaf like nanostructure electrode for high performance supercapacitor and quantum-dot sensitized solar cells. *Appl. Surface Sci.* **2018**, *435*, 666–675. [[CrossRef](#)]
28. Kim, H.J.; Kim, J.H.; Pavan Kumar, C.H.S.S.; Punnoose, D.; Kim, S.K.; Gopi, C.V.V.M.; Rao, S.S. Facile chemical bath deposition of CuS nano peas like structure as a high efficient counter electrode for quantum-dot sensitized solar cells. *J. Electroanal. Chem.* **2015**, *739*, 20–27. [[CrossRef](#)]
29. Rao, S.S.; Durga, I.K.; Varma, C.V.T.; Punnoose, D.; Cheol, L.J.; Kim, H.J. The synthesis and characterization of lead sulfide with cube-like structure as a counter electrode in the presence of urea using a hydrothermal method. *New J. Chem.* **2015**, *39*, 7379–7388. [[CrossRef](#)]
30. Zhang, Y.; Tian, J.; Li, H.; Wang, L.; Qin, X.; Asiri, A.; Al-Youbi, A.; Sun, X. Biomolecule-Assisted, Environmentally Friendly, One-Pot Synthesis of CuS/Reduced Graphene Oxide Nanocomposites with Enhanced Photocatalytic Performance. *Langmuir* **2012**, *28*, 12893–12900. [[CrossRef](#)] [[PubMed](#)]
31. Page, M.; Niitsoo, O.; Itzhaik, Y.; Cahen, D.; Hodes, G. Copper sulphide as a light absorber in wet-chemical synthesized extremely thin absorber (ETA) solar cells, *Energy Environ. Sci.* **2009**, *2*, 220–223. [[CrossRef](#)]
32. Wang, Y.; Zhang, X.; Chen, P.; Liao, H.; Cheng, S. In situ preparation of CuS cathode with unique stability and high rate performance for lithium ion batteries. *Electrochim. Acta* **2012**, *80*, 264–268. [[CrossRef](#)]
33. Wei, W.; Mi, L.; Gao, Y.; Zheng, Z.; Chen, W.; Guan, X. Partial ion-exchange of nickel-sulfide-derived electrodes for high performance supercapacitors. *Chem. Mater.* **2014**, *26*, 3418–3426. [[CrossRef](#)]
34. Prusty, B.; Adhikary, M.C.; Das, C.K. Synthesis of NiS anchored graphenenanocomposites: High performance supercapacitor electrode material. *Int. J. Curr. Res.* **2014**, *6*, 7448–7452.
35. Xia, H.; Zhu, D.; Luo, Z.; Yu, Y.; Shi, X.; Yuan, G.; Xie, J. Hierarchically Structured Co<sub>3</sub>O<sub>4</sub>@Pt@MnO<sub>2</sub> Nanowire Arrays for High-Performance Supercapacitors. *Sci. Rep.* **2013**, *3*, 2978. [[CrossRef](#)] [[PubMed](#)]
36. Chen, C.; Zhang, Q.; Peng, C. Facile Synthesis of Core-shell Structured CuS@PANI Microspheres and Electrochemical Capacitance Investigations. *Polym. Polym. Compos.* **2017**, *25*, 483–488.
37. Beka, L.G.; Li, X.; Liu, W. Nickel Cobalt Sulfide core/shell structure on 3D Graphene for supercapacitor application. *Sci. Rep.* **2017**, *7*, 2105. [[CrossRef](#)] [[PubMed](#)]
38. Han, H.; Bu, Y.G.; Xiong, W.L. Construction of Complex CoS Hollow Structures with Enhanced Electrochemical Properties for Hybrid Supercapacitors. *Chem* **2016**, *1*, 102–113.
39. Nazish, P.; Sajid, A.A.; Hatem, R.A.; Moo, H.C. Facile Synthesis of SnS<sub>2</sub> Nanostructures with Different Morphologies for High-Performance Supercapacitor Applications. *ACS Omega* **2018**, *3*, 1581–1588.

